

13 Jan 2005

**Proposal for a Forward Meson Spectrometer
For STAR**

**S. Heppelmann, L. Eun, G. Rakness, J. Passaneau
Penn State University**

**L.C. Bland, R.L. Brown, A. Ogawa
Brookhaven National Laboratory**

**F. Bieser, H.J. Crawford, J. Engelage, E.G. Judd, C. Perkins
University of California, Berkeley/Space Sciences Institute**

**A.A.Derevschikov, V.I. Kravtsov, Yu.A.Matulenko, A.P.Meschanin,
D.A.Morozov, L.V.Nogach, S.B.Nurushev, K.E.Shestermanov, A.N.Vasiliev
IHEP Protvino**

**J.L. Drachenberg, C.A. Gagliardi
Texas A&M University**

**Draft proposal to be submitted to NSF Major
Research Instrumentation (MRI) Solicitation**

Table of Contents

Project Description.....	3
What do We Know About Gluon Densities in Nuclei? Parton Model at Small x.....	5
Parton Saturation and Macroscopic Gluon Fields	5
Early Results from RHIC	8
Proton Spin with the FMS	9
FMS in Heavy Ion Physics	10
FMS Configuration	11
High Voltage Distribution	12
Trigger and Readout Electronics	13
Plan for Measurements.....	14
Management Plan.....	15
Impact of Infrastructure.....	17

Project Description

The theory that describes electromagnetic phenomena, Quantum Electrodynamics (QED), has its origin in the description of macroscopic electric and magnetic fields, Maxwell's equations. These equations of macroscopic phenomena are the basis of the early theory of radiation that led to Planck's hypothesis of quantized action and thereby to quantum mechanics. The theory of the color force, Quantum Chromodynamics (QCD), describes the dynamics of individual partons that are equivalent to the "test particles" of electromagnetic theory. QCD does not yet have an analog of Maxwell's equations for macroscopic color fields. Recent evidence from the Relativistic Heavy Ion Collider (RHIC) at Brookhaven National Laboratory (BNL), however, may lead to such an extension, and perhaps to a fundamental shift in our understanding of the color force in the nucleus.

This is a proposal to construct a Forward Meson Spectrometer (FMS) for use at the Solenoidal Tracker at RHIC (STAR) [1] to enable measurement of the gluon distribution, $xg(x)$, in nuclei in the range $0.001 < x < 0.1$. The function $g(x)$ gives the probability to find gluons, the carriers of the strong force, with a fraction x of the longitudinal momentum of the parent proton (Fig. 1) or neutron. We propose to construct the FMS from existing lead-glass cells to cover the range $2.5 < \eta < 4.0$ (polar angle range $2.1 < \vartheta < 9.4^\circ$), giving STAR nearly hermetic electromagnetic coverage in the range $-1 < \eta < 4$ ($2 < \vartheta < 130^\circ$). The FMS will allow correlation measurements between forward mesons and photons with signals from the full STAR detector, including the electromagnetic calorimeters and the forward and midrapidity time-projection chambers (TPC). Exploiting the capabilities of the RHIC accelerator and the existing STAR detector, and using simple 2-body kinematics, the FMS allows measurement of the gluon density in protons and in nuclei down to $x \sim 0.001$.

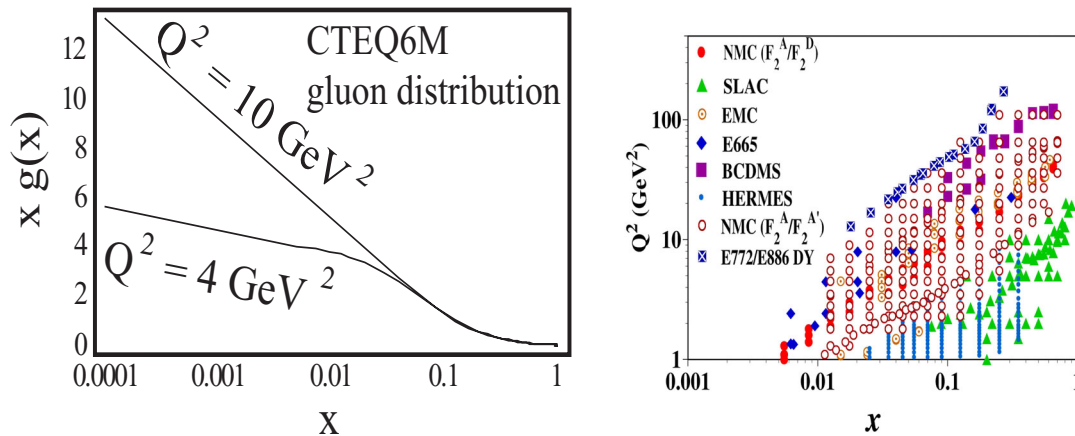


Figure 1 Left: Recently published nucleon gluon distributions [4]. Note the rapid rise in $xg(x)$ for $x < 0.01$, a discovery made at HERA based on studies of deep inelastic scattering (DIS), using electron(positron)+proton collisions at $\sqrt{s}=300 \text{ GeV}$ [22,23]. Right: Values of DIS kinematic variables x and Q^2 where nuclear data from only fixed-target DIS experiments at much lower \sqrt{s} constrains the nuclear gluon density for $x > 0.02$ [6,7].

With the addition of the FMS, STAR will be able to achieve three important physics objectives. The first is a measurement of the parton model gluon density distributions, $xg(x)$, in gold nuclei for $0.001 < x < 0.1$. The second involves the characterization of expected gluon saturation effects in these measurements as input to new models for macroscopic gluon fields. The third involves measurements with transversely polarized protons that will resolve longstanding questions about the origin of very large transverse spin

asymmetries in $p_{\uparrow} + p \rightarrow \pi^0 + X$ reactions initiated by transversely polarized proton beams for forward π^0 production.

From comprehensive measurements of p+p, d+Au, and Au+Au interactions, STAR and the other RHIC experiments (PHENIX, BRAHMS, PHOBOS) strongly suggest that the central collisions of two gold nuclei at $\sqrt{s}=200$ GeV lead to a new form of matter that appears opaque to high momentum hadrons [2]. It is believed that this dense matter evolves from an initial state involving the collision of the soft gluon fields of each nucleus [3]. The nuclear gluon field distribution might naively be expected to result from a convolution of the gluon density distributions of all the individual nucleons. While the nucleon gluon density distributions are determined by global fits to data [4,5], the nuclear gluon distribution in the region of small x ($x < 0.02$) is not yet known [6,7]. There is indirect experimental evidence from RHIC [8] that the small x gluon distribution in a large nucleus like gold will be reduced, or shadowed, from the nominal superposition of the distributions of the included protons and neutrons, a phenomenon described as saturation [9-18].

In d+Au collisions, the FMS will face the d beam and will see neutral pions (π^0) produced by large- x quarks in the deuteron interacting with the low- x gluons in the Au nucleus. The analysis will require detection of a second particle in coincidence with a triggering particle in the FMS, typically a photon or a π^0 . The coincident signal might be a high momentum track or jet detected in the STAR TPCs or it might be a photon or π^0 detected in the barrel (BEMC) or endcap (EEMC) calorimeters. For $x < 0.01$, the coincident particle will be a second π^0 or photon detected in the proposed FMS. The spatial dependence of the nuclear gluon density [19,20] will be determined by measuring particle multiplicities in the Au beam direction using existing subsystems of STAR.

Analysis of the kinematics of the relative momentum between the trigger particle and the coincident particle allows us to determine $g(x)$ in the Au nucleus. This density measurement provides the essential input to the simulation codes that can determine the energy density achieved in the collision of two heavy nuclei, the state which might expand to become the quark gluon plasma.

The same correlated particle analysis will allow us to study the physics of the saturation region. This physics is associated with the transformation from a parton-dominated picture of the nuclear gluon distribution to a picture for which macroscopic QCD fields might provide the appropriate physics description. With the FMS the azimuthal angle of separation between the two pions will be measured. The peak at 180° , the classic signature of two-parton interactions, is expected to broaden or disappear when scattering from macroscopic gluon fields dominates scattering from single gluons.

The analysis of FMS-triggered data at STAR will also be used in polarized proton running. The electromagnetic calorimetry over the full acceptance, $-1 < \eta < 4$, will greatly enhance the spin program where the goal is to understand how quark and gluon fields conspire to share the proton's $1/2$ unit of spin. Polarized Deep Inelastic Scattering (DIS) experiments found that the intrinsic spin of quarks and antiquarks contribute only $\sim 20\%$ to the nucleon spin, contrary to early theoretical expectations of $>60\%$. A RHIC spin program objective is to understand how gluon spin and orbital angular momentum play a role in this "missing spin puzzle". The correlated pion analysis of the FMS will play a crucial role in answering these questions and might lead to a resolution of the longstanding question about the origin of the large transverse single spin asymmetry in forward pion production.

What do We Know About Gluon Densities in Nuclei? Parton Model at Small x

For 20 years, a central objective in high energy physics has been the systematic characterization of parton (quark and gluon) density distributions. Groups like CTEQ (Fig. 1) [4,5] have collected data from relevant experiments with a goal of determining the parton densities within the proton. From factorization theorems we know that there is a class of high-transverse-momentum two-parton (leading twist) experiments that can be understood in terms of an initial state of independent partons within a proton. In this factorization picture, the part of the cross section due to a particular sub-process is equal to the product of a calculable parton-level cross section and the two universal initial state parton probability densities

$$\sigma(x_n, x_m) \propto \sigma_{nm} f_n(x_n) f_m(x_m).$$

The parton densities $f(x)$ are universal properties of the proton, applicable in all hard scattering processes, and in most cases (but not all) refer to the positive definite probability density to find a parton “ n ” ($n=q$ for quark, \bar{q} for antiquark and g for gluon, with $f_g(x)$ referred to as $g(x)$) carrying a fraction “ x ” of the parent nucleon longitudinal momentum; x is a kinematic variable in deep inelastic scattering (DIS). We combine contributions from all partonic sub-processes that lead to the same final state and account for contributions that come from all possible x values by adding the partial cross sections.

The nucleon gluon distributions $xg(x)$ are known in the region $0.001 < x < 0.01$ (left panel of Fig. 1) but the nuclear distributions are not. Our present understanding of how parton distribution functions (PDFs) are changed when nucleons are bound in a nucleus is primarily derived from DIS of charged leptons from nuclear targets. The charged leptons used in DIS interact with the electrically charged quarks, not the electrically neutral gluons, and provide measurements of structure functions, F_i . In the parton model, $F_2(x, Q^2) = x \sum_n e_n^2 [q_n(x, Q^2) + \bar{q}_n(x, Q^2)]$, where e_n^2 is the squared electric charge of the quark of type n and Q^2 is the squared four momentum transfer of the scattered lepton, equated to the square of the scale at which the parton substructures are observed. Gluon densities are determined from the QCD evolution equations [21] applied to scaling violations of the F_2 structure function measured for the nucleon over an extremely large x and Q^2 range at the HERA collider [22,23]. Sensitivity to $g(x)$ in DIS is approximately given by the Q^2 variation of F_2 at half that x value, $g(2x) \propto \partial F_2(x, Q^2) / \partial(\ln Q^2)$ [24]. The kinematic range of the world data for the gluon distribution in nuclear targets is shown in the right panel of Fig. 1 as used in a recent global analysis of nuclear modifications to parton distribution functions [6,7]. Such input to the nuclear gluon density is available only for $x > 0.02$ because nuclear DIS is restricted to fixed target experiments. As will be discussed below, the study of $d(p)+Au$ collisions at $\sqrt{s_{NN}}=200$ GeV can provide direct sensitivity to the nuclear modification of the gluon density for x values on the order of $x \sim 0.001$ and can test the universality of the nuclear gluon density in the range $0.02 < x < 0.1$. Comparable sensitivity in DIS to such low x would require an electron-ion collider [25].

Parton Saturation and Macroscopic Gluon Fields

In the parton model, factorization theorems allow us to add cross sections rather than quantum amplitudes, with partons considered quantum mechanically independent of each another. Within this picture, we are tempted to imagine that the gluon distribution of a nucleus might be obtained by adding the gluon distributions for each nucleon, with some accounting for the relative motion of the nucleons in the nucleus. While perhaps true for large x processes, at small x the uncertainty principle tells us that the partons will all overlap in the longitudinal direction, so the partons do not interact independently. The front surface partons will interfere or shadow the back surface partons of the nucleus. For more than 20 years it has been recognized [16] that the quantum independence of partons cannot extend to very small x where the gluon density is very large.

To determine the density scale at which collective behavior may become evident, one imagines that a scattering process at fixed p_T will probe a transverse area approximately given by $S(p_T) = \pi(\hbar/p_T)^2$. For example at $p_T = 2$ GeV/c, this corresponds to about 0.3 mb. In comparison to the proton cross sectional area of about 30 mb, this is small. The number of gluons that are present and that could shadow one another above x is nominally given by $n_{gluons}(x) = \int_x^1 g(x')dx'$. At $x=0.01$ $n_{gluons} \approx 7$, increasing by 7–8 for each order of magnitude decrease in the lower limit of x . At $x=0.001$, the product of cross section times number of gluons is $S(2 \text{ GeV}/c) \times n_{gluons}(0.001) \approx 5$ mb. While this calculation is little more than dimensional analysis, the result suggests that for events with these kinematics, the chances of finding more than one gluon within the transverse resolution of the scattering probe is less than 20 %. However in nuclei, the area of the nucleus grows roughly as $A^{2/3}$ while the number of gluons would nominally grow proportionally to A . Thus, the transverse density of nucleons should grow by a factor like $A^{1/3}$. For Au, this factor of 6 in transverse density suggests that shadowing could be substantial. By $x=0.0001$, it could become dominant. Of course, at lower p_T , the effects would show up at a larger value of x . Real predictions for the onset of shadowing vary with the model used [26], but whether shadowing modifies the gluon interactions at RHIC is an experimental question which must be answered with data.

The independent parton picture is necessarily a special case. From simple quantum mechanics, we know that if we have two contributions to scattering, from either of two gluons in a proton, the cross section should depend on the sum of amplitudes with accounting for the relative phase of the initial state gluons. When the resolving power of the probe sees overlapping gluons, shadowing will occur and we say that the parton distribution has saturated. This is a signal that macroscopic fields could be a better way to describe the process.

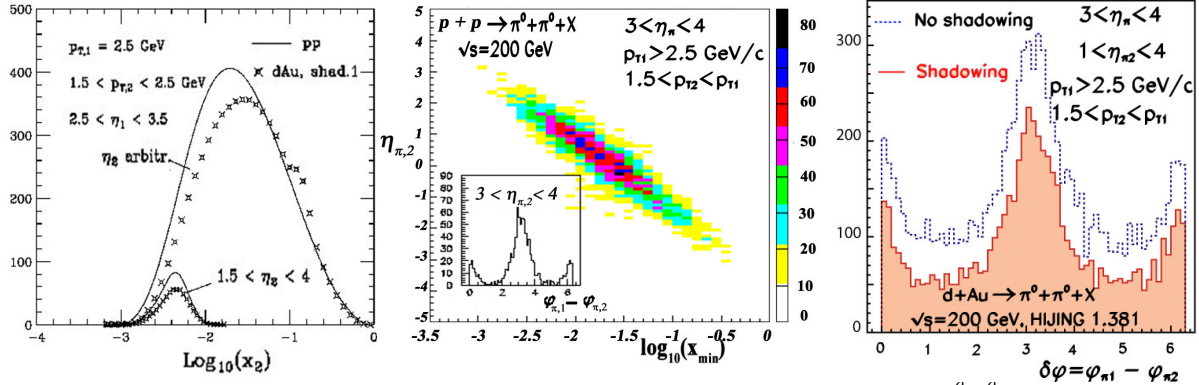


Figure 2 (Left) NLO pQCD calculation of the invariant cross sections for coincident π^0 - π^0 production at large rapidity in $p+p$ and $d+Au$ collisions at $\sqrt{s_{NN}}=200$ GeV [27]. The smallest x values are probed when both neutral pions are detected at large rapidity. (Middle) PYTHIA simulation for coincident π^0 - π^0 production at large rapidity in $p+p$ collisions at $\sqrt{s}=200$ GeV. The rapidity of the associated π^0 is strongly correlated with the x value of the soft parton involved in the partonic scattering. (Right) HIJING simulator for coincident π^0 - π^0 production at large rapidity in $d+Au$ collisions at $\sqrt{s}=200$ GeV. Compared to the $p+p$ simulations, the peaks in $\Delta\phi$ corresponding to elastic parton scattering, sit atop a background from other mechanisms for particle production.

As discussed in the following section, recent measurements at STAR using the prototype Forward Pion Detector (FPD) already indicate that the factorized leading twist perturbative QCD (pQCD) calculations work quite well to predict the $p+p \rightarrow \pi^0 + X$ cross section in the rapidity 3 to 4 region [28]. This gives confidence in the interpretation that at $\sqrt{s} = 200$ GeV the process is dominated by leading twist quark-gluon scattering. With the FMS focusing on π^0 pairs, we will select the small- x component shown by Next-to-Leading-Order (NLO) pQCD calculations (left panel of Fig. 2) to make only small contributions to the

inclusive measurement. The small- x component of the forward pion yield is where shadowing effects are expected to be most important [29]. In the middle panel of Fig. 2 we see that when triggering on a π^0 in the range $3 < \eta < 4$, the rapidity of the second π^0 will reflect the x of the struck gluon. The right panel of Fig. 2 shows that elastic parton scattering can be identified above physics backgrounds in d+Au collisions. Accessing the low- x gluon density in the gold nucleus by detection of π^0 - π^0 or γ - π^0 coincidences that involve a large rapidity γ/π^0 would provide complementary information to an earlier proposal to study J/ψ production in d+Au collisions [30].

There has been considerable recent interest among the experts in the application of pQCD in reconciling the meaning of shadowing with the idea of universal (factorizable) parton distributions. What has emerged recently [31] is a better understanding of just what the universal parton density means at small x . The present understanding is that the “shadowed” small x distributions should be universal but do not strictly reflect the probability for finding a parton. Included in the universal factorized functions are built-in final-state correlations with other gluons in the proton. We now see that even from the strict, leading twist perspective, low x perturbation theory has a different interpretation from large x because it always involves a sampling of the macroscopic gluon fields. In light of this, there is real excitement that a variety of low x phenomena from shadowing to large transverse spin asymmetries may be tied together with pQCD in ways not before appreciated.

In the spirit of Maxwell’s Equations, QCD models are now emerging that predict relationships between the soft gluon fields and the source color-charge distributions. Measurements of gluon shadowing at RHIC and the LHC will be essential input for models that predict the relationships between quark distributions and macroscopic gluon fields.

Among the descriptions of shadowing or saturation effects is the Color Glass Condensate (CGC) [16-18], an effective field theory aimed at understanding parton saturation. In the CGC picture, the saturation effects are associated with a new phase of the gluon field. The onset of this phase is associated with measurements at small x and at small Q (related to the produced parton mass and the transverse momentum p_T associated with the scattering). Mapping out the boundaries for saturation signatures for back-to-back jet correlations as a function of x and p_T , as shown in Fig. 3, is a primary mission of the FMS.

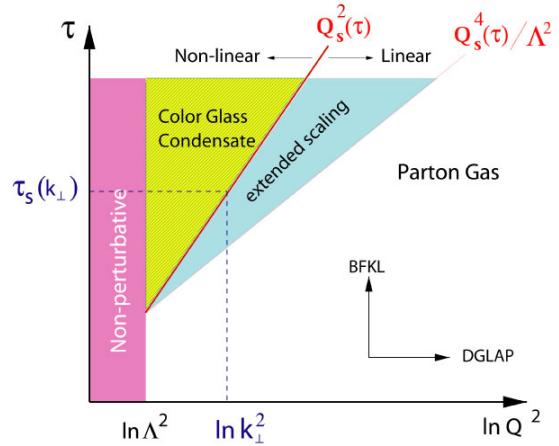


Figure 3 Diagram showing the boundary between possible “phase” regions in the $\tau=\ln(1/x)$ vs $\ln(Q^2)$ plane [11].

For p+p collisions at $\sqrt{s} \geq 200$ GeV, state-of-the-art NLO pQCD calculations quantitatively describe inclusive particle production down to p_T of ~ 2 GeV/c [32] using state-of-the-art parton distribution functions [4,5] and fragmentation functions [33,34] that describe the hadronization of the scattered partons. Furthermore, di-hadron azimuthal correlations have the same structure at these low transverse momenta as they do at the highest possible p_T values, consistent with the idea that elastic scattering of quarks and gluons is responsible for the particle production [35].

With the FMS and the barrel and endcap electromagnetic calorimeters (BEMC,EEMC), the STAR detector provides coverage that enables measurement of the x dependence of the gluon density in a heavy nucleus down to x values that are much smaller than those probed by nuclear deep-inelastic scattering measurements.

Early Results from RHIC

The first Au+Au collision runs at $\sqrt{s_{NN}}=200$ GeV resulted in the observation that high- p_T particle production at midrapidity was suppressed relative to expectations resulting from the scaling of yields from p+p collisions and that two-particle correlations were suppressed when the particles were back-to-back ($\Delta\phi\approx 180^\circ$) but not when $\Delta\phi\approx 0$ or 2π [36]. These observations are consistent with a prediction based on radiative energy loss of a high- p_T parton passing through a quark-gluon plasma [37]. A d+Au run at $\sqrt{s_{NN}}=200$ GeV was scheduled early in the RHIC program (run 3) to eliminate the possibility that this was due to initial state effects. For d+Au collisions, midrapidity particle production was found to have a small enhancement, consistent with the Cronin effect [38], and back-to-back correlations more closely resembled results from p+p collisions than from Au+Au collisions. Hence, the suppression of back-to-back correlations in Au+Au collisions was attributed to the strongly interacting matter formed by those collisions.

Measurements made by the BRAHMS collaboration during the d+Au RHIC run [8] showed that inclusive particle production was suppressed in these collisions as the rapidity of the observed particles increased. This provided a hint that the gluon distribution in the Au nucleus is depleted at low- x .

It is easy to understand how this suppression can occur within the standard pQCD picture of particle production. In that picture, the quarks and gluons each carry a fraction of their parent hadron momentum given by x . They elastically scatter and then fragment to the final state hadrons observed with a given transverse momentum (p_T) and at a given scattering angle (ϑ). The angle is related to their pseudorapidity by $\eta = -\ln \tan \vartheta/2$. For collinear parton pairs, it is easily shown that

$$x_+ \approx \frac{p_T}{\sqrt{s}} (e^{+\eta_1} + e^{+\eta_2}) \xrightarrow{\eta_1 \gg \eta_2} x_F \quad x_- \approx \frac{p_T}{\sqrt{s}} (e^{-\eta_1} + e^{-\eta_2}) \xrightarrow{\eta_1 \gg \eta_2} x_F e^{-(\eta_1 + \eta_2)},$$

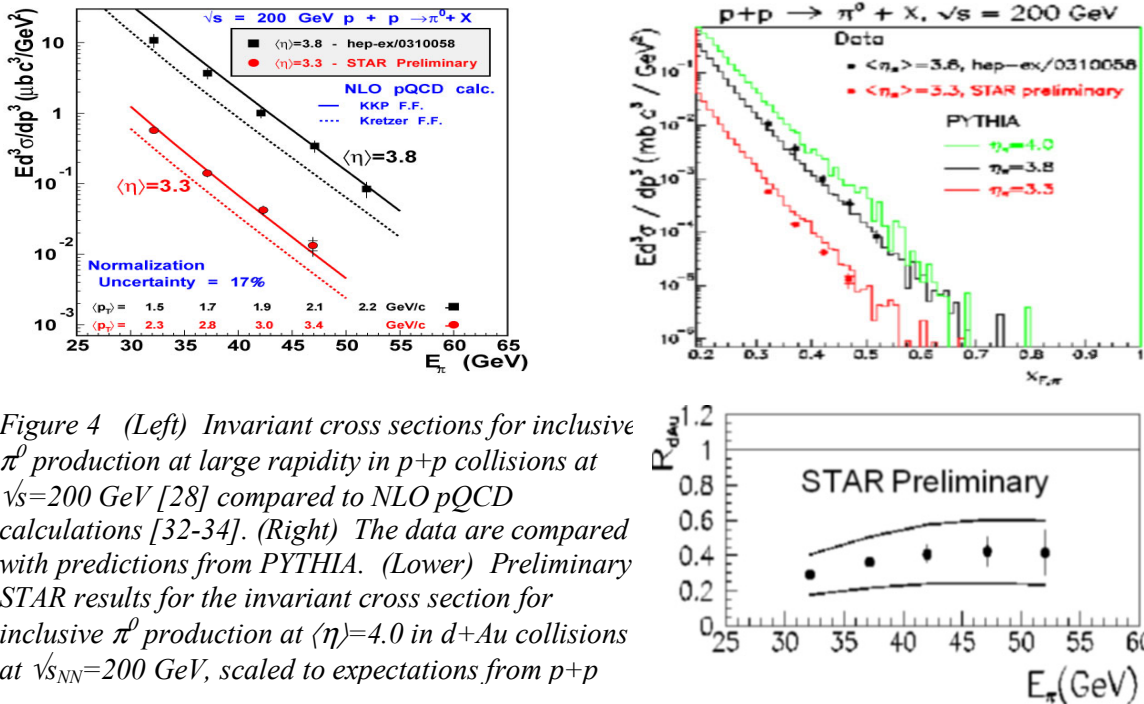


Figure 4 (Left) Invariant cross sections for inclusive π^0 production at large rapidity in p+p collisions at $\sqrt{s}=200$ GeV [28] compared to NLO pQCD calculations [32-34]. (Right) The data are compared with predictions from PYTHIA. (Lower) Preliminary STAR results for the invariant cross section for inclusive π^0 production at $\langle\eta\rangle=4.0$ in d+Au collisions at $\sqrt{s_{NN}}=200$ GeV, scaled to expectations from p+p

where the Feynman- x variable is introduced ($x_F = 2p_L/\sqrt{s}$), and p_L is the longitudinal momentum

component of the detected particle. For inclusive particle production, one of the two hadrons is observed at η_1 and the second hadron has a broad η_2 distribution and $\Delta\phi\approx 180^\circ$. By detecting a high energy hadron at large η_1 , initial states with a large- x parton (most probably a quark) and a low- x parton (most probably a gluon) are selected. For each unit rapidity increase, the average x of the parton from the initial state parent hadron is decreased by e^* . Hence, the observed suppression of particle production at increasing rapidity can be interpreted as a reduction in the probability of finding gluons in the gold nucleus at small x .

The BRAHMS results [8] were confirmed in measurements by PHENIX [39]. The STAR collaboration also made measurements of large rapidity particle production and produced a limited data sample for two-particle correlations involving a large rapidity particle [35]. These data were obtained with an electromagnetic calorimeter (FPD) positioned close to the beam. The topology of the energy deposition in the FPD allows for robust identified π^0 measurements, including its energy and direction. Since the π^0 is a pseudoscalar particle, kinematic distributions of its diphoton decay are exactly calculable in any frame of reference. Hence, calibrations of the FPD response can be obtained at the level of $\sim 1\%$ simply by requiring a fully consistent response of all cells of the calorimeter to the photons produced by the $\pi^0 \rightarrow \gamma\gamma$ decay. The preliminary results for the inclusive cross section for π^0 production in d+Au collisions, scaled by the cross section in p+p collisions, is shown in Fig. 4. This figure also shows that the simulation code PYTHIA is able to reproduce the absolute cross section of the produced π^0 from p+p collisions giving us a tool to guide the design of the FMS and the interpretation of the data.

Proton Spin with the FMS

Our understanding of the two-particle correlations involving large rapidity particles, and our ability to use these correlations to measure nuclear gluon distributions, is a direct result of the methodology developed to understand the first spin asymmetry measurements at RHIC. It is no surprise that the FMS will be a powerful tool in studying the spin structure of the proton.

An early prediction of pQCD was that, at leading twist and with collinear factorization, the chiral properties of the theory would make the analyzing power, A_N , for particles produced with transversely polarized proton beams small [40]. From AGS energies [41] to Fermi Lab energies [42] and most recently at STAR[28] (see Fig. 5), a large transverse spin analyzing power has been observed for the production of pions at large rapidity. The consistent trend is that the asymmetry in $p_\uparrow + p \rightarrow \pi^0 + X$ increases rapidly for Feynman x above about 0.3. Transverse single spin asymmetries have also been observed in semi-inclusive DIS from polarized targets [43] and experimental studies of these spin effects is a quite active area of research. The FMS is ideally suited to extend these studies.

One view of this physics emerges from calculations of twist-3 contributions [44] to the asymmetry. These calculations provide terms that may be related to macroscopic gluon fields in the polarized nucleon. There are multiple phenomenological effects that have been identified as possible sources for the large asymmetries, but only two that are expected to be large. One is the Sivers effect [45,46], which is an initial state correlation between the parton intrinsic transverse momentum k_T and the transverse spin of the nucleon. In the Sivers framework, A_N is sensitive to the contribution of quark orbital angular momentum to

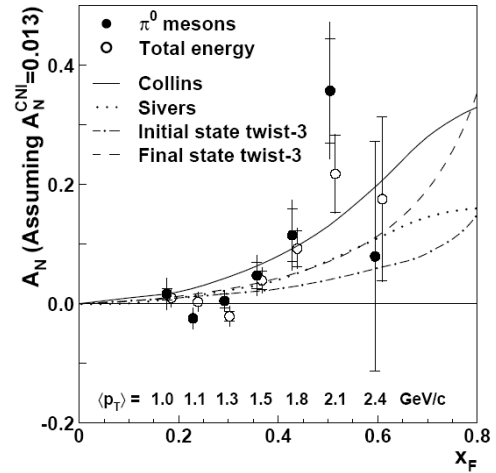


Figure 5 STAR measurement of transverse asymmetry for π^0 production.

* A similar decrease in x is a consequence of studying particle production in collisions at higher \sqrt{s} .

the nucleon spin. Here the large transverse asymmetries are the result of a spin dependent p_T trigger bias in the particle production favoring events where k_T is in the same direction as p_T .

While the Sivers effect connects A_N to the orbital angular momentum of quarks, the second effect, called the Collins effect [47,48], is directly sensitive to the transversity structure of the quark, the transverse polarization of quarks (and antiquarks) in a transversely polarized proton. Here the quark scatters, preserving its transverse spin, and then fragments into pions and other hadrons. The fragmentation function reveals the polarization of the fragmenting quark and thus the initial quark state. In this example, the asymmetry does not appear in the jet production directly, but only in the fragmentation. The jet axis would not show the transverse asymmetry, but a pion fragment would. Recent calculations that include the full k_T dependence in the convolution integrals may provide some indication that the Collins effect is small [49].

If the Sivers effect is present, we can further characterize the effect with a measurement of the away side jet. Measurement of the difference in transverse momentum of these two back-to-back jets, or their surrogates, will depend upon k_T of the struck quark. The asymmetry in this k_T measurement is exactly what the Sivers model predicts [50].

The FMS will be able to distinguish between these mechanisms. By looking at pairs of same-side neutral pions, we can measure the asymmetry as a function of the two pion kinematics. With the FMS we will separately measure the contributions to this asymmetry that comes from the jet axis vs. that which comes from the jet structure. Many theory papers have studied this problem: however, the need for data is great. The FMS STAR experiments on transverse polarization will provide to theorists the necessary input to determine the relative contributions from the Sivers effect and the Collins effect.

The technique of detecting coincident neutral pion pairs will also be used in p+p collisions to study gluon polarization via measurement of double longitudinal spin asymmetries. The PHENIX collaboration has already presented their initial results for $\pi^0 A_{LL}$ at midrapidity [51]. A NLO pQCD analysis [52] of the midrapidity cross section [53] indicates that midrapidity π^0 production in the p_T range where A_{LL} is measured has large contributions from both gluon-gluon and quark-gluon scattering. In contrast, the forward π^0 production favors the quark-gluon over the gluon-gluon subprocess and has the advantage of utilizing the very high polarization of the valence quark. Valence quarks are found highly polarized in polarized DIS; the “missing spin puzzle” refers to the integral over all x of the quark and antiquark contributions. Dominance of quark-gluon scattering provides better sensitivity to the sign of the gluon polarization since terms quadratic in the gluon polarization are small. The forward π^0 measurements will reach lower x , and even lower with planned $\sqrt{s} = 500$ GeV collisions. Furthermore $\pi^0 - \pi^0$ measurements with wide rapidity coverage of the STAR BEMC, EEMC and FMS will provide a strong constraint on gluon polarization as a function of x .

The universality of polarized PDFs can be tested by selecting quark-quark scattering in longitudinally polarized p+p collisions and comparing A_{LL} measurements with polarized DIS measurements. This universality test is very important to validate future global analyses that will include data from longitudinally polarized p+p collisions aimed at determining gluon polarization.

FMS in Heavy Ion Physics

With the discovery of jet quenching in Au+Au interactions, a significant fraction of the STAR analysis is now devoted to correlations among high p_T particles. These rely at present on the TPC and will soon include the full Barrel EMC and the Endcap EMC, allowing coverage with tracking and calorimetry from $-1 < \eta < 2$. It is known from the beam-beam counters that the particle multiplicity in the forward direction is likely to

be too large to allow isolation and reconstruction of individual π^0 from central Au+Au collisions in the FMS. However, our simulations have shown that we can accomplish this for less central Au+Au collisions and for central collisions of lighter systems, such as Cu+Cu, which are being investigated as part of the program to characterize the new form of matter. In addition to allowing us to measure inclusive π^0 and perhaps heavy meson cross sections over a limited range in centrality, extending STAR's reach out to $\eta \sim 4$, we expect to be able to contribute to the particle identified analysis of collective effects such as the hydrodynamic flow that is helping to elucidate the equation of state of the excited matter.

FMS Configuration

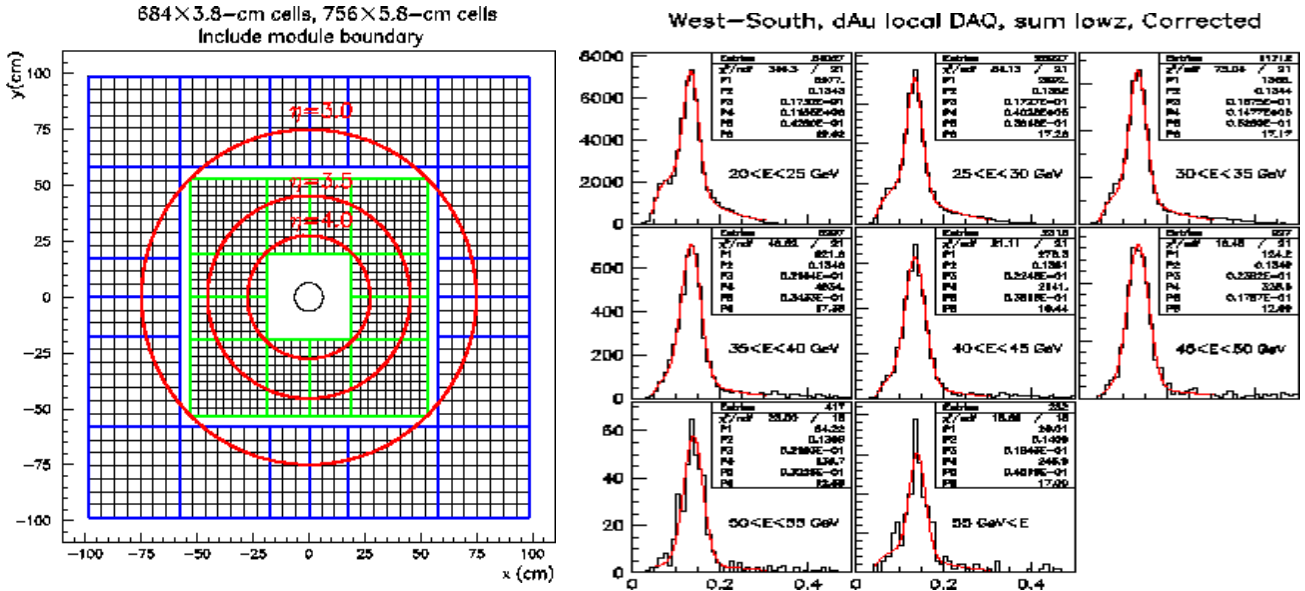


Figure 6 (Left) Schematic of proposed FMS layout as seen from the STAR interaction point looking to the west. The FMS is comprised of an inner calorimeter and outer calorimeter that surround the beam, mounted at a longitudinal distance of 7.5m from the STAR interaction point. The inner calorimeter (IC) is made from a square annulus of 3.8 cm x 3.8 cm x 45 cm optically isolated lead-glass cells, each viewed by a FEU-84 photomultiplier tube. The outer calorimeter (OC) is made from a square annulus of 5.8 cm x 5.8 cm x 60 cm optically isolated lead-glass cells, each viewed by a XP2202 photomultiplier tube. The resulting FMS has an areal coverage of 2 m x 2 m. (Right) Di-photon invariant mass distributions measured for d+Au collisions at $\sqrt{s_{NN}}=200$ GeV with the STAR FPD at $\langle \eta \rangle = 4.0$. The FPD has the same cell size as the IC of the FMS and is positioned 8.0m from the interaction point. Robust π^0 identification is demonstrated for energies up to 60 GeV.

The STAR Forward π^0 Detector (FPD) is in a sense the prototype for the proposed Forward Meson Spectrometer. The FPD demonstrates the feasibility of large rapidity measurements with electromagnetic calorimetry in both p+p collisions and d+Au collisions at $\sqrt{s_{NN}}=200$ GeV at RHIC. Each FPD calorimeter is a 7x7 matrix of 3.8cm x 3.8cm x 45cm lead-glass cells from IHEP, Protvino that can be positioned in the range $3.3 < \eta < 4.0$. The FMS increases the areal coverage of forward calorimetry at STAR by more than a factor of 25, thereby allowing studies of $\gamma-\pi^0$ and $\pi^0-\pi^0$ correlations. By implementing the FMS in STAR, the study of $\gamma-\pi^0$ and $\pi^0-\pi^0$ correlations in both rapidity and azimuthal angles is enabled over a very broad range of rapidity, from $-1 < \eta < 4$. Furthermore, the large area of the FMS allows inclusive measurements of π^0, γ production over a broad range of η and p_T , kinematic variables that are related to the τ and Q^2 variables of Fig. 3, and should allow the measurement of inclusive production of heavier mesons. A schematic of the proposed FMS detector is shown in Fig. 6, along with examples of the mass resolution

from a topological analysis [54] of the energy deposition for data obtained with the cells configured in the current FPD.

The FMS will provide complete azimuthal coverage for the pseudorapidity interval $2.5 < \eta < 4.0$ and will be built from existing lead-glass cells. The $3.8 \text{ cm} \times 3.8 \text{ cm} \times 45 \text{ cm}$ lead glass cells of the inner calorimeter will come from the 162 cells of the existing FPD calorimeters mounted on the west side of the STAR magnet, supplemented by an additional 500 cells from IHEP, Protvino. Each cell will be viewed by an existing FEU-84 photomultiplier tube, energized by a Cockcroft-Walton base described below. The outer calorimeter is built from 800 cells of $5.8 \text{ cm} \times 5.8 \text{ cm} \times 60 \text{ cm}$ Schott F2 lead glass cells that comprised the inner calorimeter of FNAL-E831. Each cell will be viewed by a Photinis XP2202 photomultiplier tube, energized by a Cockcroft-Walton base.

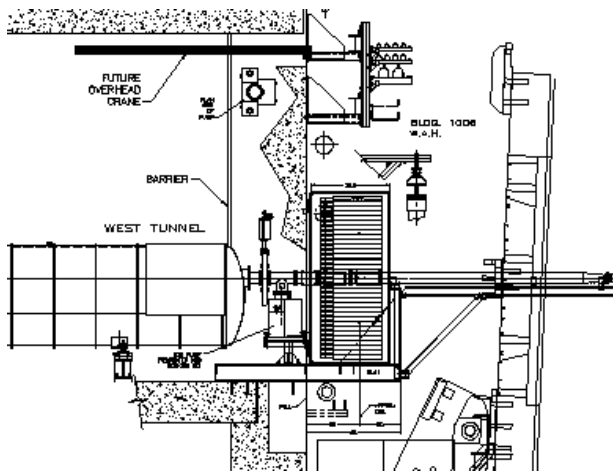


Figure 7 Elevation view of the west side of the STAR Wide Angle Hall (WAH). The FMS is mounted at the opening of the RHIC tunnel into the west side of the STAR WAH. The location shown is 7.5 m from the STAR interaction point.

The 1440 lead glass cells will be grouped into submodules, and the submodules will be stacked into two light-tight enclosures that will allow the calorimeter halves to be moved along a rail system away from the beam pipe for access to vacuum-system hardware and for maintenance of the calorimeter. The weight of the calorimeter cells above the beam will be supported by a square central hub, split along a vertical center line for the two calorimeter halves. Figure 7 shows a schematic of the mounting of the FMS at the opening of the RHIC tunnel into the west side of the STAR Wide Angle Hall (WAH). For d+Au runs, the deuteron beam goes from right to left in this figure. The FMS will be assembled by transporting calorimeter submodules through the RHIC tunnel to its opening on the west side of the STAR WAH. Further details are provided below.

High Voltage Distribution

The phototube high voltage will be provided with Cockcroft-Walton style bases to be developed and fabricated at Penn State. Similar bases have been successfully used in many experiments. This option has several advantages over resistive bases, including simplification of cabling and low power consumption. The heat load within the detector enclosure will be minimal, as the steady state power dissipation for similar Cockcroft-Walton bases has usually been less than 0.1 W/channel or about 150 W for the entire FMS detector. Following the lead of other groups, we will distribute power and digital control in a simple daisy chain cable configuration from one or more digital controllers. The voltages will be set and checked periodically by the controller. The basic starting point for our design of the Cockcroft-Walton bases is that which was used in the Zeus calorimeter [55]. The second generation of Zeus bases was upgraded and fabricated at Penn State by John Passaneau. Communication between the controller and the bases will be a serial link. In Zeus, this link was a very basic implementation of TCP/IP protocol. As with the Zeus system, this choice allowed for the possibility that the system could be controlled by a DC power supply and a generic computer. It is based on experience at Penn State with the Zeus Cockcroft-Walton bases that we have estimated the cost of design and fabrication of the FMS voltage system.

Two types of bases will be required for the FMS, one to support the 684 FEU-84 photomultiplier tubes that make up the center of the detector and another for the 756 Photinis XP2202 photomultiplier tubes. Both designs will consist of similar control and oscillator sections. The number of stages in the capacitor-diode cascade and the connections between the phototube and the cascade stages will be different for the two tube types. A good solution for the FEU-84 tube was implemented in the WA98 experiment using 43 stages [56]. After completion of the base design, we anticipate several rounds of realistic tests, recognising that high voltage stability and minimal charge leakage require a careful implementation. Documentation of the design, fabrication and testing will be very complete. Extensive testing of the design will be done at Penn State before general fabrication begins.

Trigger and Readout Electronics

The electronics design is driven by the requirements of the physics goals. Briefly, these are to provide energy measurement over the accessible range at RHIC with sufficient sensitivity to lead to unambiguous π^0 mass reconstruction while simultaneously rejecting background.

1. Dynamic range (0-250 GeV) and sensitivity (0.05 GeV): We need to measure energies in a single crystal up to $x_F \sim 1$ for the 250 GeV proton beams because the minimum x for gluons is probed with maximum x_F for quarks, and because spin effects increase with x_F of the detected meson. At larger rapidities (~ 4) we will approach the highest energies where 0.25 GeV resolution is sufficient, while at lower rapidities, we will need better sensitivity (0.05 GeV) to provide mass resolution. This gives a minimum of 10 bits of dynamic range for the digitized signal. Given typical PMT gains this converts to ~ 0.5 pC per least count. Including a non-zero pedestal value to assure accuracy for small or zero pulses requires an additional 2 bits, leading to a requirement for 12 bit digitization.
2. Signal capture (~ 80 ns active capture time): Shower development within the PbGl blocks leads to photon arrival time at the PMT cathode spread over as large as 50 ns.
3. Background suppression (time stamp “hits” with an accuracy of $< \sim 5$ ns.): The detector is placed as near to the beam pipe as geometry will allow, making it susceptible to the near-beam background radiation fields. Measurements at STAR at the location planned for the FMS indicate that the background can be reduced with a timing resolution of 5 ns, while still allowing for variation in vertex location within the diamond.
4. Rate capability (operate at 10 MHz to match the STAR system): The STAR trigger is based on a fully pipelined dead-time-less operation allowing maximum use of the luminosity.

These requirements cannot be met by any currently available commercial electronics nor any hardware already in use at RHIC. Advances in available electronics components makes it possible to greatly improve the flexibility and performance of deadtimeless signal-capturing calorimeter instrumentation. Our design will follow the STAR hardware standards, using VME infrastructure for the digitizers and Linux based PCI infrastructure for data collection.

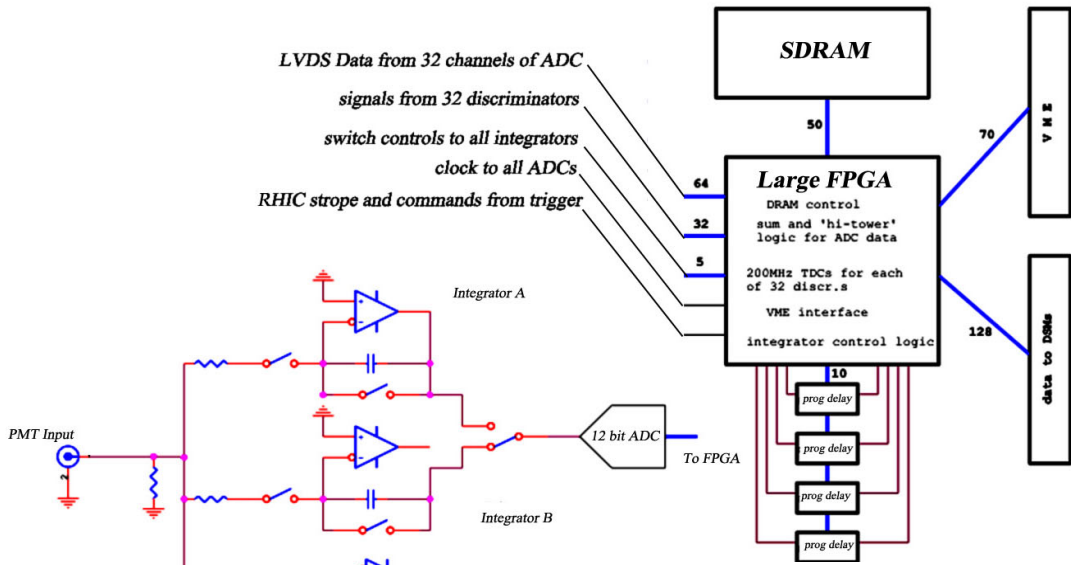


Figure 8 Block diagram of circuit and board for ADC/TDC system.

The block diagram of a single input channel is shown in Fig. 8, along with the block diagram of a 32 channel board. Each PMT feeds a separate channel. Each channel feeds both a discriminator and an integrated charge-to-digital converter (ADC).

The requirement for widely adjustable integration times has led us to develop a dual integrator front end for the ADC. One integrator is active while the other is being reset in each RHIC clock cycle of 105 ns. The integrator is alive only during a gate time whose leading and trailing edges are register selectable anywhere within the 105 ns RHIC clock period. At the leading edge of the next clock cycle the integrators are switched and the last active integrator presents its signal to the 12 bit, 40 MHz digitizer. Output from the digitizer is shipped to a Field Programmable Gate Array (FPGA) for packaging.

Output from the discriminator is used as input to a 5 ns sensitivity time-to-digital-converter (TDC). The TDC is based on a counter operating at 200 MHz and counting up until the leading edge of the discriminator is seen. This leads to a 5 bit TDC value which is stored and reset at the leading edge of each RHIC clock signal.

The FPGA will route each channel's digital signals to local memory for storage until receipt of a level 0 trigger at which time all, or all non-zero, channels will be shipped via fiber optic cable to a PCI receiver card in a Linux CPU. This data acquisition system can run independently of the STAR daq or, being Linux based, can be seamlessly sewn into the STAR data stream, or both. The FPGA will also treat groups of 16 crystals as trigger patches: it will form sums of the 16 ADC values and it will select the highest of the 16 ADC values as a "high tower". It will then allow selection of any contiguous group of 6 from the sum and 6 bits from the high-tower and send these 12 bits to an existing STAR Data Storage and Manipulation (DSM) board in the trigger, exactly as done for the BEMC and EEMC.

Plan for Measurements

We know that twist 2 NLO pQCD correctly predicts the pion inclusive cross section for $p + p \rightarrow \pi^0 + X$ in the region $3 < \eta_1 < 4$ and $p_T \geq 2$ GeV/c for $\sqrt{s} = 200$ GeV collisions, unlike at lower collision energies [57]. We will now leverage that fact to measure and interpret a second π^0 from the recoil

jet. If two-body elastic parton scattering (twist 2 or leading twist) is the origin of the particle production, and secondary interactions are weak, then for $|\eta_1 - \eta_2| < 0.5$, the $\Delta\phi$ distribution will have two peaks separated by 180° whose widths carry information about momentum imbalance (k_T) and the transverse momentum associated with fragmentation (j_T); both effects are associated with multiple soft gluon emission either before or after the partonic scattering. For larger $|\Delta\eta|$, near-side correlations disappear and the $\Delta\phi$ distribution has a single peak at 180° . The η dependence of the two-particle yield can be related to the x dependence of the gluon density associated with the incident hadron having its longitudinal momentum opposite to that of the forward pion. Hence, the modification of the gluon density in a heavy nucleus with mass number A can be determined by comparison of results from p+p and d(p)+A collisions at the same $\sqrt{s_{NN}}$ for comparable final-state observables. If a saturated gluon state is present, suppression of the nuclear cross section will occur and the $\Delta\phi$ peak at 180° will be broadened and reduced [58]. In the extreme saturation limit, a monojet is produced [59] and the η distribution of the recoil hadrons provides detailed information about the dense gluon medium probed by the high- x parton from the deuteron (proton).

As shown in Fig. 2, pQCD calculations [27] suggest that the lowest x values for the gluon density are probed when both jets from the elastic parton scattering are produced at large rapidity. Both $\pi^0 + \pi^0$ and $\pi^0 + \gamma$ final states can be analyzed in the FMS. The large size of the proposed FMS enables the use of isolation cuts to distinguish between π^0 decay photons and direct photons. The dominant subprocess for direct photon production at RHIC is QCD Compton scattering, $qg \rightarrow \gamma q$, which can also be used to directly probe the small x gluon density with only minimal physics backgrounds from other partonic scatterings. The left panel of Fig. 2 shows the x distribution of gluons that contribute to the inclusive measurement and how the small x component is selected by coincident detection of two neutral pions both in the forward direction. The middle panel of Fig. 2 shows a PYTHIA 6.222 simulation [60] for the rapidity correlation of $\pi^0 - \pi^0$ coincidences and demonstrates how this measurement will unfold the x distribution from the inclusive measurement. The p_T of the π^0 must be large enough to favor elastic parton scattering over inelastic scattering [35] although both contributions are contained in PYTHIA and NLO pQCD calculations. Finally, the right panel of Fig. 2 shows a HIJING 1.381 [61] simulation of 750 million minimum-bias events, from which all $\pi^0 - \pi^0$ pairs with the specified p_T and η are selected and used to compute $\Delta\phi$. Unlike the case for p+p collisions, the elastic parton scattering peaks in the $\Delta\phi$ distribution sit atop a background from the nuclear collision. Despite the background, the elastic parton scattering is readily discriminated and can be identified as the expected peak in $\Delta\phi$. We can quantitatively describe these distributions from $1 < \Delta\phi < 5.28$ radians by a Gaussian function, used to model the peak, and a constant background. A best fit to the $\Delta\phi$ distribution in Fig. 2 results in $\sim 2.3 \times 10^3$ events in the peak for simulations done without shadowing and $\sim 1.8 \times 10^3$ events in the peak for the simulations done with shadowing. We can expect that a 10-week d+Au run will allow us to sample $> 6 \times 10^{10}$ minimum-bias interactions, based on RHIC performance for d+Au collisions achieved in the last weeks of run 3. Accounting for detector efficiencies for the FMS and endcap EMC, the detectors covering $1 < \eta < 4$, the simulations suggest we will observe at least 8×10^3 events in the $\Delta\phi$ peak without shadowing. This is enough to investigate the spatial dependence of the nuclear gluon density [19,20] using particle multiplicity measurements in the Au beam direction made by other STAR subsystems to determine sensitivity to the impact parameter of the collision.

Management Plan

The FMS project includes design, fabrication, installation and operation of the spectrometer at STAR. We expect to support all analysis from existing sources outside of this proposal. Infrastructure required to support the FMS at STAR will be provided by BNL operations. PSU will be the lead institution for the FMS project, acting as the liaison to the NSF. In broad terms PSU will take responsibility for PMT bases

and FMS mechanical, LBL for front-end electronics, data acquisition and triggering, and BNL and partially IHEP for installation and operation. All will share in simulation, calibration, and analysis. Here we present a time-line and some details of the management plan.

The FMS fabrication is expected to begin in July 2005. As shown in Fig. 9, milestones include delivery of PbGl to BNL, prototype electronics and base tests, calibration of individual cells, delivery of tested electronics, completion of cave infrastructure, installation of FMS at STAR, and delivery of first d+Au collisions. The year of the d+Au run is not yet finalized, although, as indicated in the accompanying letters from BNL management (Appendix XX), the run is likely in FY07 and nearly certain by FY10. Spin physics measurements can begin as soon as the FMS installation is complete. Some discussion of schedule details should help clarify our plans.

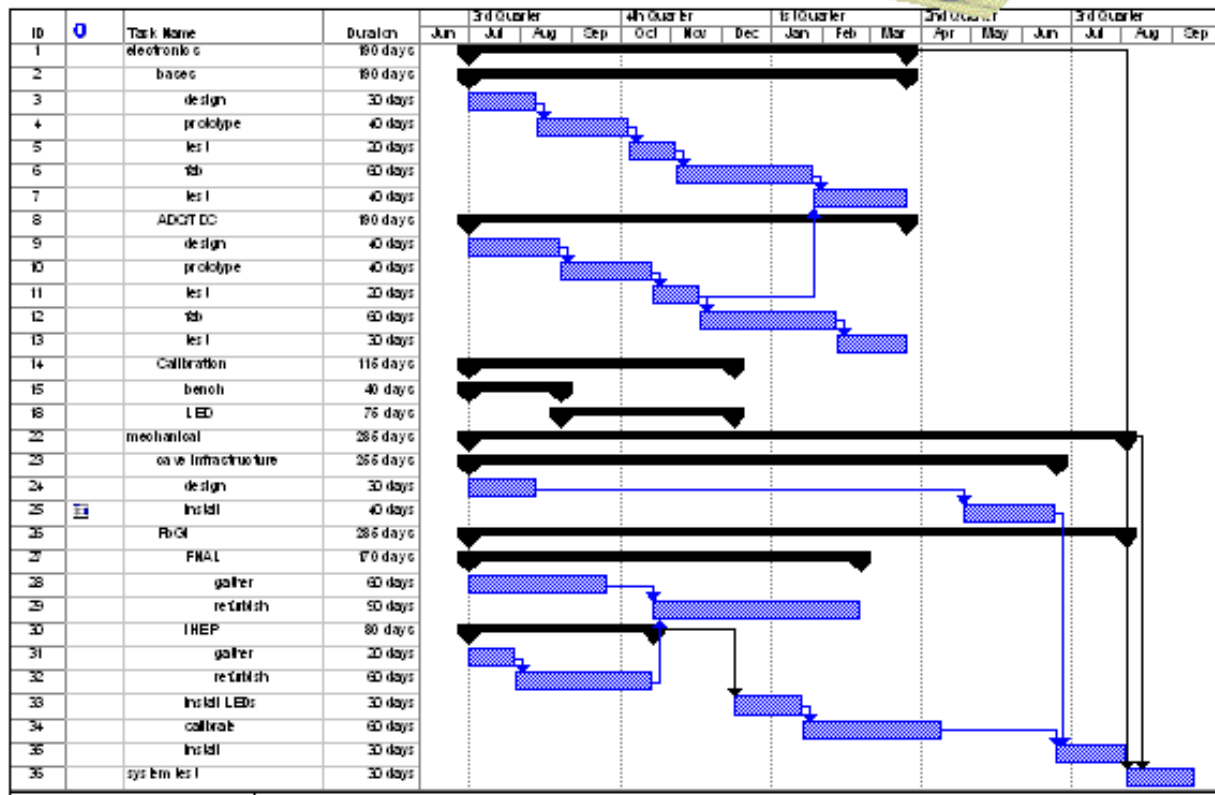


Figure 9 FMS Project Timeline

The FMS consists of 1440 cells of lead glass (PbGl), 684 small and 756 large cells. These are being contributed by Protvino and BNL (through FNAL and Colorado). Mechanical means to hold the internal structure of the array will be designed and built at PSU funded by this proposal. Support for the array and facilities for mounting the detector in the STAR cave will be provided by BNL operations.

Each cell is viewed by a photomultiplier tube (PMT): 684 model FEU-84 are supplied by IHEP with the PbGl, and 756 Photinis XP-2202 will be acquired for the FNAL-E831 inner calorimeter. Each requires a high-voltage chain (base) to develop a signal on the anode which is sent via RG58 cable to the 50Ω input of an ADC/TDC. The base is to consist of a Cockroft-Walton circuit designed and built by PSU staff and tested by PSU students. The ADC/TDC system and all DAQ electronics are designed and fabricated at LBL under this proposal. Initial testing of each ADC/TDC board will be done at LBL in part by students using existing STAR electronics test facilities there. The boards will then be sent to PSU for tests with calorimeter cells as part of the testing procedure for each base.

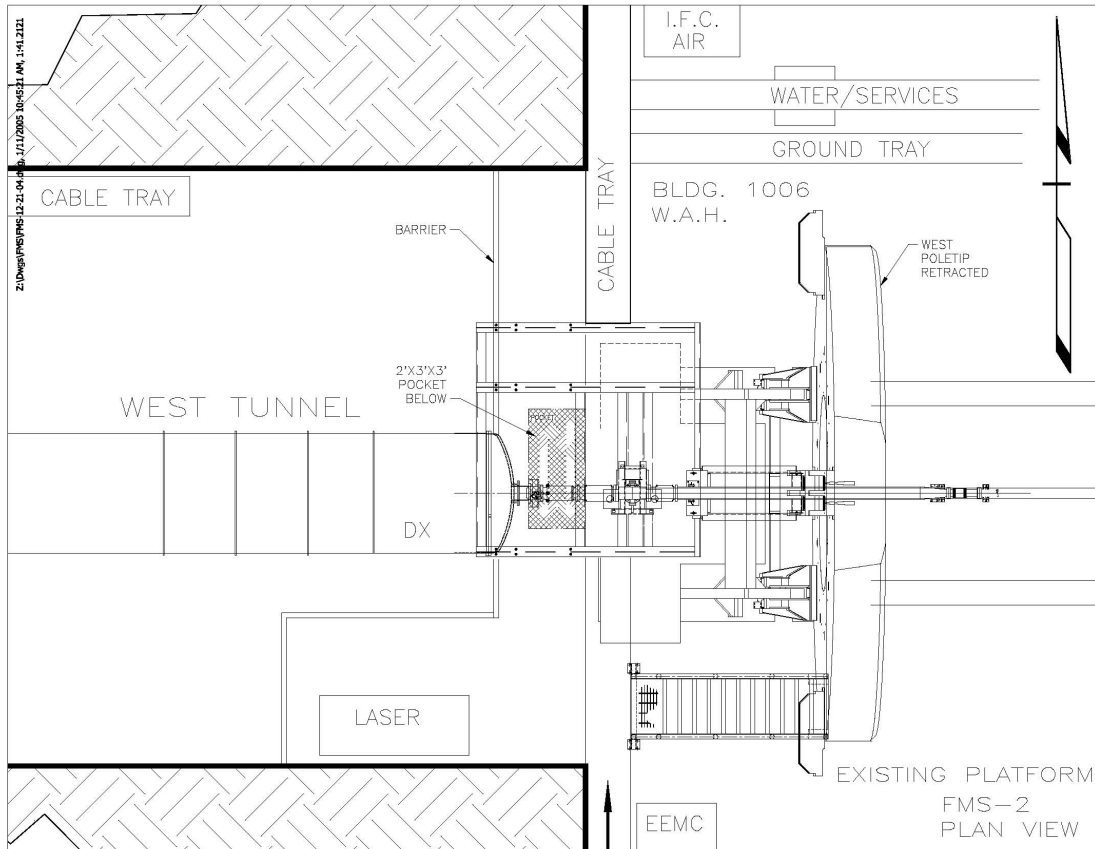


Fig.10: Existing west tunnel area with STAR west pole tip in retracted position. The existing platform extension is approximately 8" above tunnel floor height.

A full test setup at PSU is provided under this proposal: it will be used in the parts testing and in the analysis software development by PSU students. BNL will take primary responsibility for calibration of each cell and stacking/installing the calorimeter in the STAR cave. TAMU is expected to aid in these activities, primarily through student support. There are two systems for calibration, in addition to the final step in which parameters are tweaked to minimize variance in reconstructed pion mass. The first step, designed and implemented by BNL through this proposal, will consist of cell by cell calibration on the bench using a single LED source with a monitor PMT to normalize results. This will be supplemented by a system consisting of an LED mounted on each cell to be fired periodically during data taking. This LED system is to be designed and built at LBL and funded through this proposal.

Our internal organization is typical of any small collaboration, very tight communications and general group consensus building. Final decisions will lie with the majority among the principal investigators. Official contact is through our primary investigator at PSU.

Impact of Infrastructure

The proposed Forward Meson Spectrometer at STAR will reside on the west RHIC tunnel extension in the WAH, Bldg. 1006. The location of this 10-ton lead glass detector that will clamshell in two pieces around the vacuum beam pipe, is on the IR side of the DX magnet. The proposed operating location of this detector will affect existing RHIC/STAR infrastructure such as vacuum pumping systems, existing

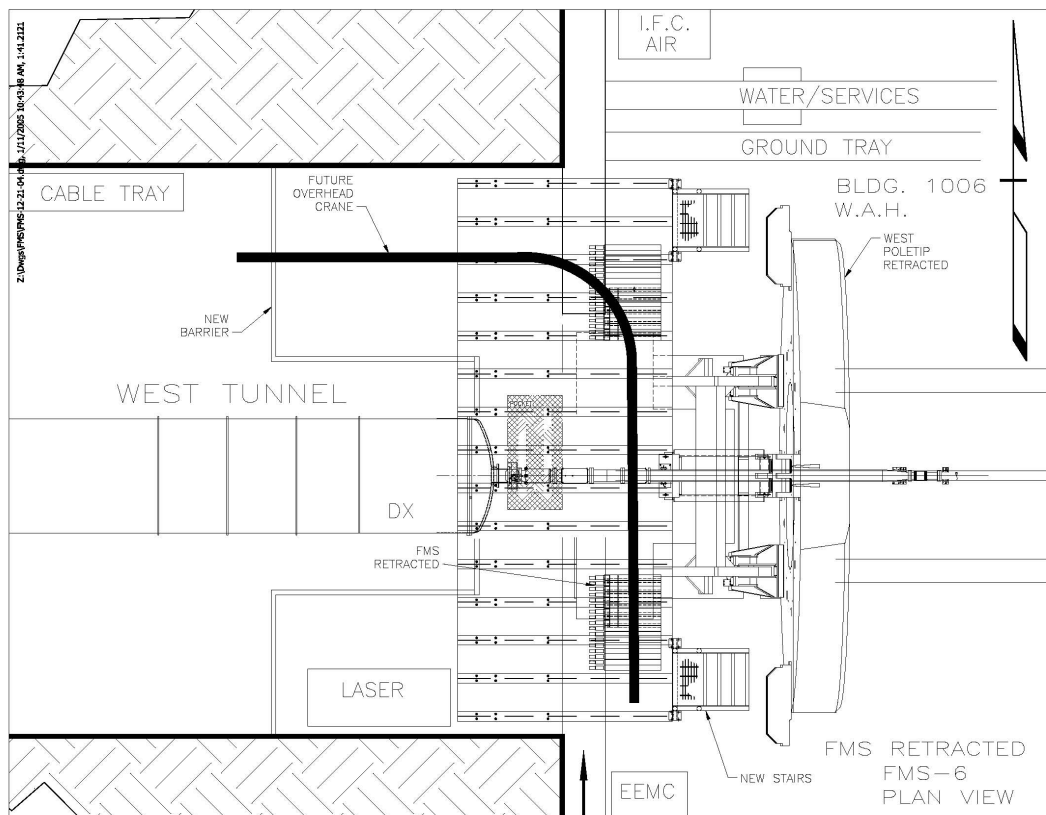


Fig. 11: Plan view of proposed modifications of west tunnel infrastructure. The FMS detector is shown separated into two halves in their maintenance locations.

tunnel platform extension into the WAH, the tunnel ODH security barrier, and cable tray utility runs on the west wall of the WAH. Fig.1 below shows a plan view of the existing area of the west tunnel WAH at Bldg. 1006.

The existing vacuum ion pump located on the platform extension will have to be relocated and hard coupled to the DX vacuum valve and will require a smaller physical sized pump and stand. The BPM position will be closer to the IR and a new vacuum spool piece extension maybe required. A new vacuum beam pipe support design is required since the location of the FMS detector interferes with the existing turnbuckle support system. The existing platform extension is anchored into the tunnel concrete floor and cantilevered into the WAH by approximately 4-ft. It is not structurally adequate to support the 10-ton detector load or does it have sufficient width for separating the two halves of the new FMS detector. The proposed platform extension will be the width of the tunnel opening and flush with the floor of the tunnel. It will be supported from the floor of the WAH by columns and have two, north and south, access stairs to the tunnel from the WAH floor. The plan is to install the lead glass as multiple unit bundles banded together in modules weighing less then 1-ton. Since the platform extension and the location of the FMS detector is not within WAH crane coverage a new over crane rail and trolley chain hoist will be installed from the tunnel ceiling and span over the platform extension area of the detector. Detector lead glass modules will be brought into the area by way of the RHIC tunnel from 7 o'clock access and carted to the 6 o'clock area. The existing ODH security barrier will be stepped back into the tunnel, as was modified on the south west side, to allow additional space for working on the experimental side of the barrier. Modules will be rigged from the tunnel with the trolley chain hoist and assembled on their slide bases on the platform extension either side of the vacuum beam pipe. Fig. 2 shows the proposed configuration of the west tunnel area.

Each detector half will be installed in a light tight box and mounted to a linear slide base with rails tracking north and south on the platform extension, orthogonal to the beam pipe. Two full height single 19” electronics racks will reside on the floor of the WAH north and south of the platform extension in support of detector electronics crates. AC power will have to be routed to these new rack locations. Existing tray utilities that now span across the tunnel opening will have to be rerouted below the platform extension so as not to interfere with chain hoist operation. New cable tray will have to be installed in support of the existing EEMC detector and the proposed FMS detector.

The following is an engineering estimate for both detector related items and infrastructure modifications and does not include the cost of system electronics, cable connectors, and cables. It is assumed that the labor cost of engineering, designer, technician, and trades are captured within C-A/STAR operating budgets and are not included in this estimate

FMS Detector Costs (included in budget table in NSF MRI proposal):

1. Readout electronics.....	300 K\$
2. High voltage distribution.....	225 K\$
3. Phototubes.....	150 K\$
4. Cabling and connectors.....	70 K\$
5. Detector enclosures and glass module packaging.....	35 K\$
6. Electronics racks fully equipped.....	15 K\$
7. Crating & shipping of lead glass.....	5 K\$
Sub-total:.....	800 K\$

Infrastructure Costs (non-NSF sources):

1. Slides and rail system.....	25 K\$
2. Platform extension.....	25 K\$
3. Vacuum system modifications.....	32 K\$
4. Vacuum pipe support.....	15 K\$
5. Crane rail & chain hoist.....	11 K\$
6. Platform access stairs.....	3 K\$
7. ODH security barrier modification.....	2 K\$
8. Cable tray modifications.....	5 K\$
9. AC power routing.....	3 K\$
Sub-total:.....	121 K\$
Total.....	921 K\$
20% contingency.....	184 K\$

References

- [1] K.H. Ackermann *et al.* (STAR collaboration), Nucl. Instrum. Meth. **A499** (2003) 624.
- [2] “*Experimental and Theoretical Challenges in the Search for the Quark Gluon Plasma*” (STAR collaboration) [nucl-ex/0501009]; “*Formation of dense partonic matter in relativistic nucleus-nucleus collisions at RHIC*” (PHENIX collaboration), [nucl-ex/0410003]; “*Quark Gluon Plasma and Color Glass Condensate at RHIC?*” (BRAHMS collaboration), [nucl-ex/0410020]; “*The PHOBOS Perspective on Discoveries at RHIC*” (PHOBOS collaboration), [nucl-ex/0410022].
- [3] Miklos Gyulassy and Larry McLerran, RBRC Scientific Articles Vol. 9 (nucl-th/0405012).
- [4] J. Pumplin, D.R. Stump, J. Huston, H.L. Lai, P. Nadolsky, W.K Tung, JHEP **0207** (2002) 012.
- [5] A.D. Martin, R.G. Roberts, W.J. Stirling and R.S. Thorne, Eur. Phys. J **C28** (2003) 455.
- [6] M. Hirai, S. Kumano, T.-H. Nagai, Phys. Rev. **C70** (2004) 044905.
- [7] ” *PDFs, Shadowing and pA Collision*”, working group contribution to the CERN Yellow Report on Hard Probes in Heavy Ion Collisions at the LHC (HIP-2003-40/TH), K.J. Eskola (editor) [hep-ph/0308248]; and K.J. Eskola, H. Honkanen, V.J. Kolhinen and C.A. Salgado [hep-ph/0302170].
- [8] I. Arsene *et al.* (BRAHMS collaboration), Phys. Rev. Lett. **93** (2004) 242303.
- [9] J.-P. Blaizot, F. Gelis and R. Venugopalan, Nucl. Phys. **A743** (2004) 57; Nucl. Phys. **A743** (2004) 13.
- [10] Edmond Iancu and Raju Venugopalan, review for Quark Gluon Plasma 3, R.C. Hwa and X.-N. Wang (eds.), World Scientific, 2003 [hep-ph/0303204].
- [11] Adrian Dumitru and Jamal Jalilian-Marian, Phys. Rev. Lett. **89** (2002) 022301.
- [12] L. McLerran and R. Venugopalan, Phys. Rev. **D49** (1994) 3352.
- [13] A.H. Mueller and A.I. Shoshi, Nucl. Phys. **B692** (2004) 175.
- [14] A.H. Mueller, Nucl. Phys. **A724** (2003) 223.
- [15] A.H. Mueller, Nucl. Phys. **B643** (2002) 501.
- [16] L.V. Gribov, E.M. Levin and M.G. Ryskin, Phys. Rept. **100** (1983) 1.
- [17] A.H. Mueller and Jian-wei Qiu, Nucl. Phys. **B268** (1986) 427; J.-P. Blaizot and A.H. Mueller, Nucl. Phys. **B289** (1987) 847.

- [18] L.D. McLerran and R. Venugopalan, Phys. Rev. **D49** (1994) 2233; (1994) 3352; **D50** (1994) 2225.
- [19] L. Frankfurt, M. Strikman and S. Liuti, “*Parton Distributions in Hard Nuclear Collisions*” prepared for 4th RHIC Workshop on Experiments and Detectors for a Relativistic Heavy Ion Collider (1990) 103.
- [20] V. Emel’yanov, A. Khodinov, S.R. Klein and R. Vogt, Phys. Rev. C **61** (2000) 044904.
- [21] Yu.L. Dokshitzer, Sov. Phys. JETP **46** (1977) 641; V.N. Gribov and L.N. Lipatov, Sov. Jorun. Nucl. Phys. **15** (1972) 438 and 675; G. Altarelli and G. Parisi, Nucl. Phys. **B126** (1977) 298.
- [22] C.Adloff *et al.* (H1 Collaboration), Eur. Phys. J. **C21** (2001) 33 [hep-ex/0012053]. I. Abt *et al.* (H1 collaboration), Nucl. Phys. **B407** (1993) 515.
- [23] S. Dhekanov *et al.* (ZEUS Collaboration), Eur. Phys. J. **C21** (2001) 443 [hep-ex/0105090]. M. Derrick *et al.* (ZEUS collaboration), Phys. Lett. **B316** (1993) 412.
- [24] K. Prytz, Phys. Lett. **B311** (1993) 286.
- [25] A. Deshpande, R. Milner and R. Venugopalan, *The Electron Ion Collider: A high luminosity probe of the partonic substructure of nucleons and nuclei* BNL report 68933 (2002).
- [26] Leonid Frankfurt, Vadim Guzey and Mark Strikman, J. Phys. **G27** (2001) R23 [hep-ph/0010248].
- [27] V. Guzey, M. Strikman and W. Vogelsang, Phys. Lett. **B603** (2004) 173 [hep-ph/0407201].
- [28] J. Adams *et al.* (STAR collaboration), Phys. Rev. Lett. **92** (2004) 171801 [hep-ex/0310058].
- [29] R. Vogt, Phys. Rev. C (in press) [hep-ph/0405060].
- [30] S.R. Klein and R. Vogt, Phys. Rev. Lett. **91** (2003) 142301.
- [31] S. Brodsky, P. Hoyer, N. Marchal, S. Peigne, F. Sannino, Phys. Rev. **D65** (2002) 114025.
- [32] F. Aversa *et al.*, Nucl Phys. **B327** (1989) 105; B. Jager *et al.*, Phys. Rev. **D67** (2003) 054005; and D. de Florian, Phys. Rev. **D67** (2003) 054004.
- [33] B.A. Kniehl, G. Kramer and B. Poetter, Nucl Phys. **B597** (2001) 337.
- [34] S. Kretzer, Phys. Rev. **D62** (2000) 054001.

- [35] A. Ogawa (for the STAR collaboration), submitted talk presented at the 12th International Workshop on Deep Inelastic Scattering (DIS2004) [hep-ex/0408004].
- [36] C. Adler *et al.* (STAR collaboration), Phys. Rev. Lett. **90** (2003) 082302.
- [37] M. Gyulassy and M. Plümer, Phys. Lett. **B243** (1990) 432; X.N. Wang and M. Gyulassy, Phys. Rev. Lett. **68** (1992) 1480.
- [38] D. Antreaysan *et al.*, Phys. Rev. **D19** (1979) 764.
- [39] S.S. Adler *et al.* (PHENIX collaboration), submitted to Phys. Rev. Lett. [nucl-ex/0411054].
- [40] G.L. Kane, J. Pumplin and W. Repko, Phys. Rev. Lett. **41** (1978) 1689.
- [41] R.D. Klem *et al.*, Phys. Rev. Lett. **36** (1976) 929; W.H. Dragoset *et al.*, Phys. Rev. **D18** (1978) 3939; S. Saroff *et al.*, Phys. Rev. Lett. **64** (1990) 995; B.E. Bonner *et al.*, Phys. Rev. **D41** (1990) 13; K. Krueger *et al.*, Phys. Lett. **B459** (1999); C.E. Allgower *et al.*, Phys. Rev. **D65** (2002) 092008.
- [42] B.E. Bonner *et al.* Phys. Rev. Lett. **61** (1988) 1918; D.L. Adams *et al.*, Phys. Lett. **B261** (1991) 201; Phys. Lett. **B264** (1991) 462; Z. Phys. **C56** (1992) 181; A. Bravar *et al.* Phys. Rev. Lett. **77** (1996) 2626.
- [43] A. Airapetian *et al.* (HERMES collaboration), Phys. Rev. Lett. **94** (2005) 012002.
- [44] A. Efremov and O. Teryaev, Phys. Lett. **B 150** (1985) 383; J. Qiu and G. Sterman, Phys. Rev. **D59** (1998) 014004; Y. Koike, AIP Conf. Proc. **675** (2003) 449.
- [45] D.Sivers, Phys. Rev. **D41** (1990) 83; **43** (1991) 261.
- [46] M. Anselmino, M. Boglione and F. Murgia, Phys. Lett. **B362** (1995) 164; M. Anselmino and F. Murgia, Phys. Lett. **B442** (1998) 470.
- [47] J. Collins, Nucl. Phys. **B396** (1993) 161; J. Collins, S.F. Heppelmann and G.A. Ladinsky, Nucl. Phys. **B420** (1994) 565.
- [48] M. Anselmino, M. Boglione and F. Murgia, Phys. Rev. **D60** (1999) 054027.
- [49] M. Anselmino, M. Boglione, U. D'Alesio, E. Leader and F. Murgia, contribution to the 16th International Spin Physics Symposium (to be published) [hep-ph/0412236]; M. Anselmino, M. Boglione, U. D'Alesio, E. Leader and F. Murgia, (to be published) [hep-ph/0408356].
- [50] Daniel Boer and Werner Vogelsang, Phys. Rev. **D69** (2004) 094025 [hep-ph/0312320].
- [51] S.S. Adler *et al.* (PHENIX collaboration), Phys. Rev. Lett. **93** (2004) 202002.

- [52] B. Jager, S. Kretzer, M. Stratmann and W. Vogelsang, Phys. Rev. Lett. **92** (2004) 121803; S. Kretzer, contribution to 34th International Symposium on Multiparticle Dynamics [hep-ph/0410219].
- [53] S.S. Adler *et al.* (PHENIX collaboration), Phys. Rev. Lett. **91** (2003) 241803.
- [54] A.A. Lednev, Nucl. Instrum. Meth. **A366** (1995) 292.
- [55] B. Ju, L. W. Mo and T. A. Nunamaker, The Cockcroft-Walton Photomultiplier Tube Base and the Ethernet High Voltage Controller, Report VPI-IHEP-91/1.
- [56] S. Neumaier *et. al.*, Nucl. Instrum. Meth., A 360 (1995) 593.
- [57] C. Bourrely and J. Soffer, Eur. Phys. J. **C36** (2004) 371 [hep-ph/0311110].
- [58] Jianwei Qiu and Ivan Vitev, Phys. Rev. Lett. **93** (2004) 262301.
- [59] D. Kharzeev, E. Levin and L. McLerran (to be published) [hep-ph/0403271].
- [60] T. Sjöstrand, P. Eden, C. Friberg, L. Lönnblad, G. Miu, S. Mrenna and E. Norrbin, Computer Physics Commun. **135** (2001) 238.
- [61] X. N. Wang and M. Gyulassy, Phys. Rev. **D44** (1991) 3501.